IEEE Photonics Journal
An IEEE Photonics Society Publication

Open Access

Integrated Silicon Photonics Remote Radio Frontend (RRF) for Single-Sideband (SSB) Millimeter-Wave Radio-Over-Fiber (ROF) Systems

Volume 11, Number 2, April 2019

Yeyu Tong
Chi-Wai Chow
Guan-Hong Chen
Ching-Wei Peng
Chien-Hung Yeh
Hon Ki Tsang

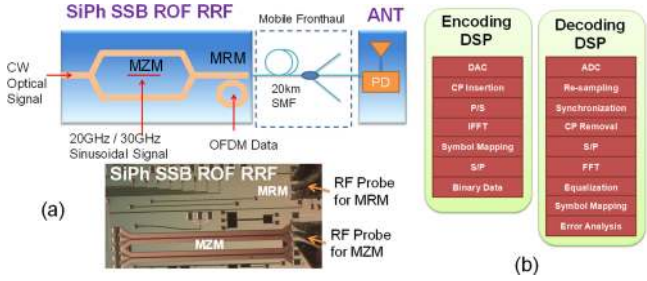

DOI: 10.1109/JPHOT.2019.2898938
1943-0655

Integrated Silicon Photonics Remote Radio Frontend (RRF) for Single-Sideband (SSB) Millimeter-Wave Radio-Over-Fiber (ROF) Systems

Yeyu Tong [1], Chi-Wai Chow [2], Guan-Hong Chen [2], Ching-Wei Peng [2], Chien-Hung Yeh [3] and Hon Ki Tsang [1]

[1]Department of Electronic Engineering, The Chinese University of Hong Kong, Hong Kong
[2]Department of Photonics and Institute of Electro-Optical Engineering, National Chiao Tung University, Hsinchu 30010, Taiwan
[3]Department of Photonics, Feng Chia University, Taichung 40724, Taiwan

DOI:10.1109/JPHOT.2019.2898938

Manuscript received January 16, 2019; revised February 2, 2019; accepted February 7, 2019. Date of publication February 12, 2019; date of current version January 4, 2019. This work was supported in part by the Ministry of Science and Technology, Taiwan, ROC, under Grant MOST-107-2221-E-009-118-MY3 and Grant MOST-106-2221-E-009-105-MY3, and in part by Higher Education Sprout Project, and the Hong Kong Research Grants Council, General Research Fund under Grant 14212816. Corresponding author: Chi-Wai Chow (e-mail: cwchow@faculty.nctu.edu.tw).

Abstract: Radio-over-fiber (ROF)-based mobile fronthaul network supporting the baseband unit and simple remote radio head is a promising network architecture for future wireless networks. In this paper, we propose and demonstrate a silicon photonics (SiPh)-based remote radio frontend (RRF) for the mm-wave ROF systems. The proposed SiPh-based RRF consisted of an integrated Mach–Zehnder modulator and a micro-ring modulator, producing a single-sideband 40 GHz millimeter-wave orthogonal-frequency-division-multiplexing ROF signal, which is robust against fiber chromatic dispersion in the mobile fronthaul transmission. The RRF is fabricated using SiPh platform and could be potentially low cost. High split-ratios can be potentially achieved. Data rate of 7.813 Gbit/s per wavelength channel is achieved in the experiment. Numerical analysis is also performed; there are good matches of the simulation and experimental results.

Index Terms: Radio-over-fiber (ROF), silicon photonics (SiPh), cloud radio access network (CRAN).

1. Introduction

Recently, due to the increase in popularity of different mobile broadband applications; the traffic capacity in radio access networks (RANs) has been growing rapidly [1]. In order to support high data rates in the future wireless and mobile systems, using higher frequency bands such as in the millimeter-wave (mm-wave) region are considered. For example, in the 5G mobile systems, apart from the 3.5 GHz carrier frequency band; mm-wave bands in 40 GHz region are considered by different countries [2]. Frequencies from 40 GHz to 100 GHz could be employed in the future fiber-wireless convergent systems [3]–[9]. When using higher frequency bands, more cell sites are required to provide satisfactory network coverage due to much higher atmospheric propagation loss during the mm-wave transmission. One of the promising architectures for supporting many cell

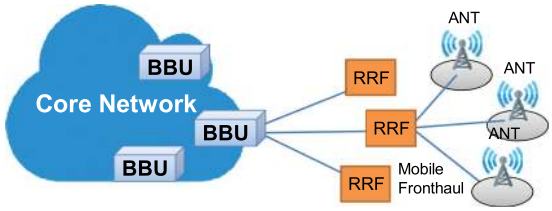

Fig. 1. CRAN architecture. ANT: antenna; BBU: baseband unit; RRF: remote radio frontend.

sites while keeping the cost down is to use the cloud radio access network (CRAN) architecture [10]–[12]. In this architecture, the traditional functions of base station (BS) will be separated into baseband unit (BBU) and remote radio head (RRH). The BBU handles the complicated functions of digital signal processing; while the RRH handles the simple emitting and receiving of wireless signals. In the CRAN, the RRH can be made simple and low-cost, facilitating its mass deployment. Existing optical fiber networks can be used to connect the RRHs and BBUs [13], and the BBUs can be migrated away from the cell cites. They can be connected in the core network (known as BBU pool) for resource sharing. In the CRAN architecture, two main signal transmission methods are proposed between BBU and RRH. They are known as digitized radio-over-fiber (ROF) [14] and analog ROF [15] signal transmission. Digitized transmissions are more favorable when the wireless carrier frequencies are low (within a few GHz), specifications such as the Common Public Radio Interface (CPRI) [16] and the Open Base Station Architecture Initiative (OBSAI) [17] are proposed and implemented. However, it is illustrated that as multiple signal streams are required to support multiple ANTs and multiple sectors per ANT in each cell site; even using the advanced digital baseband oversampled I/Q signal, ∼10 Gbit/s is required for transmitting the present 20-MHz LTE radio-frequency (RF) channel in the optical fiber [18]. Hence, it may be more impractical for using analog ROF transmission when the wireless carrier frequencies are high [19]–[20].

Silicon photonics (SiPh) technology [21] has attracted many attentions nowadays since high yield and large volume SiPh devices can be fabricated using the existing mature complementary metal oxide semiconductor (CMOS) fabrication facilities. Recently, various high performance SiPh devices can be proposed and fabricated, showing significant potential in fiber access networks [22], [23] and data center networks [24], [25].

In this work, we propose and demonstrate a SiPh based remote radio frontend (RRF) for the mm-wave analog ROF systems. The proposed SiPh based RRF consists of an integrated Mach-Zehnder modulator (MZM) and an integrated micro-ring modulator (MRM). It can produce a single-sideband (SSB) 40 GHz mm-wave orthogonal-frequency-division-multiplexing (OFDM) ROF signal. As SSB ROF signal is robust against fiber chromatic dispersion, the RRF generated SSB 40 GHz ROF signal can support a long fiber transmission (20-km) satisfying the soft-decision forward error correction (SD-FEC) threshold [26]. The proposed system can also potentially support high split-ratio at the mobile fronthaul. The high split-ratio in mobile fronthaul can facilitate the implementation of multiple-input multiple-out (MIMO) and coordinated multipoint (CoMP) techniques [27]. Numerical analysis is also performed to evaluate the proposed RRF. Good matches between the simulation and experimental results are found for the SSB 40 GHz ROF case; and good simulation transmission performance can be observed when the ROF frequency is increased to 60 GHz, suitable for the WiGig and wireless high-definition multimedia interface (HDMI) applications.

2. Architecture and Experiment

Fig. 1 shows the CRAN architecture. The BBU in the core network handles the complicated functions of signal processing; while the RRF introduced here can provide the functions of signal up-conversion. This can be implemented by generating SSB ROF signals, which are then launched into the photodiode (PD) connected to ANT for mm-wave signal emissions. The SSB ROF signals

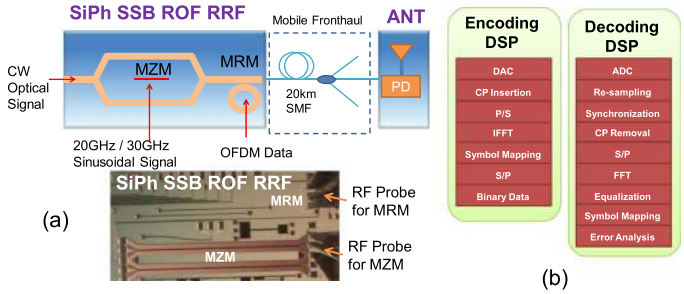

Fig. 2. (a) Proposed SiPh RRF for SSB mm-wave ROF signal generation. Inset: top-view photograph of the SiPh RRF. (b) DSP of the OFDM encoding and decoding.

are distributed from the RRF to ANTs via the mobile fronthaul network. At the PD located in the cell site, the coherent beating between the two optical tones in the ROF signal can generate mm-wave signal with frequency equals to the wavelength separation between the two optical tones. As the SSB ROF signal is used, it is robust against fiber chromatic dispersion during the mobile fronthaul transmission. In the proposed network, each RRF can connect to many ANTs. This can potentially facilitate the deployment of MIMO and CoMP [27].

Fig. 2(a) also shows the proposed SiPh RRF for SSB mm-wave ROF signal generation. A continuous wave (CW) optical signal is launched into the integrated SiPh MZM, which is electrically driven by sinusoidal signal. By basing the MZM at the transmission null point, an optical two-tone with carrier-suppressed (OTT-CS) signal can be generated. The wavelength separation between the two optical tones in the OTT-CS signal is 0.32 nm or 0.48 nm when the electrical driving signal is 20 GHz or 30 GHz respectively; producing ROF signal at 40 GHz or 60 GHz correspondingly. Then, the OTT-CS signal is launched into an integrated SiPh MRM, which is driven by the electrical OFDM signal. By launching the longer wavelength sideband of the OTT-CS signal to the resonant frequency of the MRM, it is encoded by the OFDM signal and leaving the shorter wavelength sideband un-modulated, producing the SSB ROF signal. The modulation operation of the MRM is described in [28] although the design are different from the one used in this experiment. Finally, SSB ROF signal is launched into the PD via single mode fiber (SMF) and passive fiber splitter. At the PD, the coherent beating between the modulated and un-modulated sidebands will produce the mm-wave signal carrying the OFDM data; which will be emitted by the ANT. When using 2 cascaded MZMs instead of a cascaded MZM and a MRM, the first MZM generates the OTT-CS signal and the second MZM modulates both two tones to produce the ROF signal. The advantage of using 2 MZMs is that there is no need of precise wavelength management when launching optical signal into the second MZM since MZM is wavelength insensitive. The disadvantage of using 2 MZMs is that the two tones carrying the same data will produce dispersion induced walk-off effect during mobile fronthaul transmission.

In the experiment, the optical OFDM data is encoded vi the MRM, which is connected to an arbitrary waveform generator (AWG). The AWG performs the function of digital-to-analog conversion (DAC). Fig. 2(b) illustrates the digital signal processes (DSP) used in the OFDM encoding and decoding. The OFDM signal is generated by using off-line Matlab program. The OFDM encoding DSP includes serial-to-parallel (S/P) conversion, symbol mapping, inverse fast Fourier transform (IFFT), parallel-to-serial (P/S) conversion, cyclic prefix (CP) insertion. The FFT size of 512 and CP of 1/64 are used. In this proof-of-concept experiment, the generated mm-wave ROF signal detected by the PD is directly connected to the RF-spectrum analyzer and the real-time oscilloscope (RTO) for the signal analysis. Fig. 2(b) also illustrates the DSP of the OFDM decoding, the signal is recorded by the RTO, which performs the function of analog-to-digital conversion (ADC). The OFDM decoding includes signal re-sampling, synchronization, CP removal, S/P conversion, FFT, one-tap equalization, symbol mapping, and error analysis. The bit-error-rate (BER) of the signal is obtained by measuring the signal-to-noise ratio (SNR) of the OFDM subcarriers.

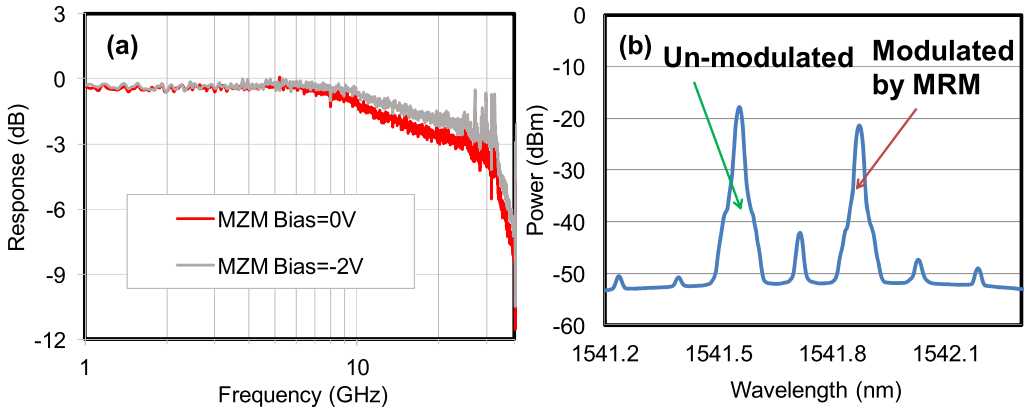

Fig. 3. Measured (a) 3-dB frequency response of MZM; and (b) optical spectrum at the output of RRF.

Inset of Fig. 2(a) shows the top-view photography of the SiPh SSB ROF RRF. In the experiment, high-speed ground-signal-ground (GSG) RF probes are used to apply the electrical sinusoidal signal to the MZM; and the OFDM data to the MRM simultaneously. The MZM and MRM are fabricated on silicon-on-insulator (SOI) substrate with a 2 μm thick buried oxide (BOX) layer and 220 nm thick top silicon layer. The MZM structure is formed by two 1.5 mm long waveguide with embedded lateral PN junctions to provide the optical phase shift. Each arm is terminated with a 25 Ω on-chip resistor, formed by two parallel 50 Ω n-doped silicon slabs between ground and signal. The MRM has the radius of 5 μm and Q-factor at zero bias of 2200. The ring-bus gap is 150 nm. Lateral PN junction is used along the ring waveguide to change the resonant frequency of the MRM for signal modulation. The optical signals launched into and out of the integrated SiPh SSB ROF RRF are via one dimensional (1-D) grating coupler (GC), which is optimized for transverse-electric (TE) polarization. The GC has uniform-period with shallow-etched. 10^{o} off-vertical coupling is used between the optical fiber and GC.

3. Results and Discussions

Fig. 3(a) shows the measured 3-dB frequency response of the MZM is 20 GHz at zero bias; and about 25 GHz at base $= -2$ V. Hence, the MZM can be electrically driven at 20 GHz to produce 40 GHz OTT-CS signal. In later analysis, it is also shown that the MZM can be driven at 30 GHz to produce 60 GHz ROF signal. When the MZM is DC-based at the transmission null, optical two tones with carrier-suppression at optical frequencies $\omega_c - \omega_m$ and $\omega_c + \omega_m$ are produced, where ω_c and ω_m are the frequencies of the optical carrier and the applied modulation respectively. Hence ROF signal of $2\omega_m$ can be produced by the coherent beating between the optical two tones. By adjusting the applied modulation, the frequency of the ROF signal produced by the RRF can be changed. In the SSB ROF signal generation, the CW optical signal at wavelength of 1541.7 nm is used. The optical spectrum at the output of the RRF is shown in Fig. 3(b), showing one sideband is un-modulated and one sideband is modulated by the MRM carrying the OFDM signal. The wavelength separation between the SSB ROF signal is 0.32 nm, corresponding to 40 GHz. After this, the optical SSB ROF signal is launched into the PD, and the coherent beating between the two sidebands can generated the 40 GHz mm-Wave signal carrying the OFDM data. Fig. 4(a) and (b) show the RF spectra measured by an RF spectrum analysis at the baseband frequency and at the 40 GHz frequency band. Although only up to 41 GHz is shown in Fig. 4(b) (limited by the frequency response of the RF spectrum analyzer), the OFDM data actually occupies frequencies from 37 to 43 GHz. The OFDM data can be successfully encoded onto the 40 GHz mm-wave signal. By switching ON and OFF the OFDM data applied to the MRM, it is observed that the extinction ratios of the OFDM data at the baseband and at 40 GHz RF band are $\sim$30 dB and $\sim$20 dB respectively.

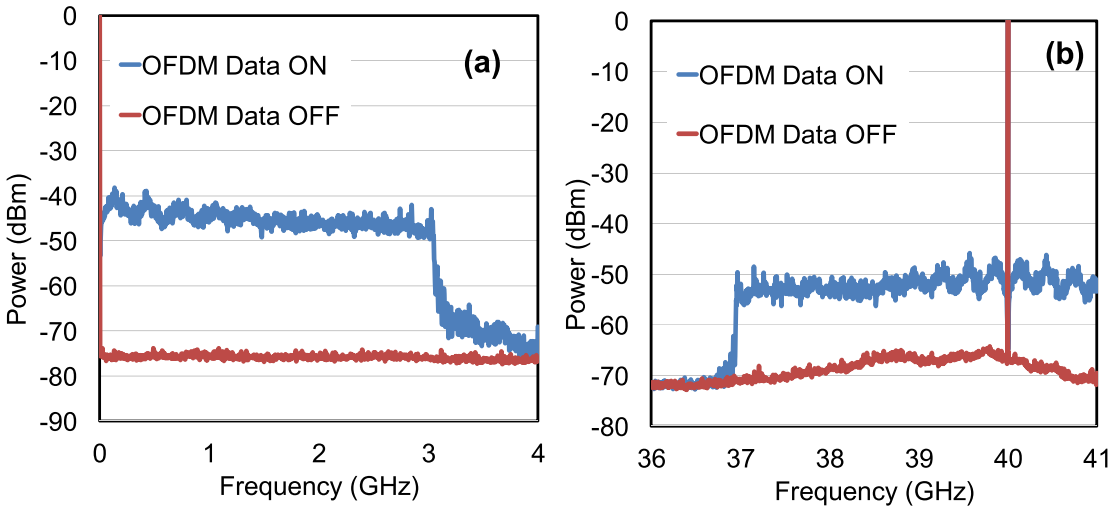

Fig. 4. Measured RF spectra of the (a) baseband frequency and (b) at the 40 GHz frequency band.

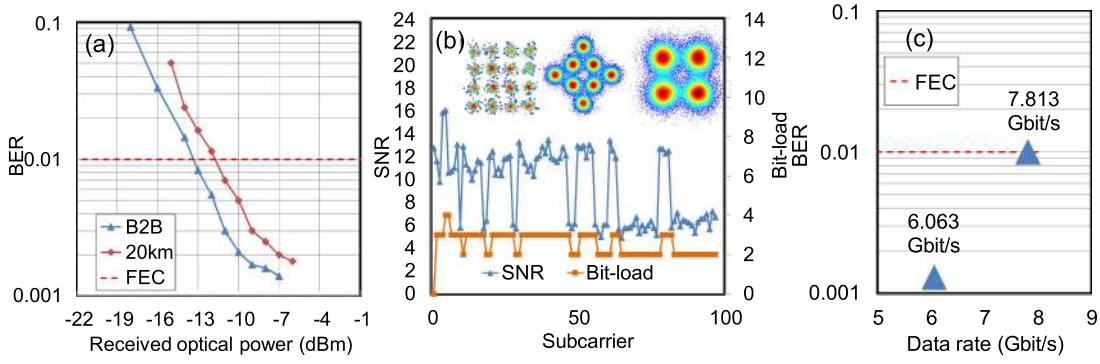

Fig. 5. (a) Measured BER at different optical power in front of the PD. (b) SNR, bit-loading and the corresponding constellation diagrams of the SSB ROF OFDM signal. (c) BER and data rate of the SSB ROF OFDM signal.

Fig 5(a) shows the measured BER performance at different received SSB ROF signal power in front of the PD. Optical launching power of +13 dBm is launched into the UE-BBU. By considering the total fiber-to-fiber loss of the SiPh RRF is ∼16 dB; 8 split-ratios can be achieved at the mobile fronthaul satisfying the SD-FEC threshold. If optical amplifier, such as semiconductor optical amplifier (SOA) with typical gain of 20 dB is used at the mobile fronthaul before the passive fiber splitter, split-ratios of 128 can be potentially achieved. Bit-loading is applied at the SSB ROF OFDM signal to increase the spectral efficiency. Fig. 5(b) shows the SNRs of different subcarriers, the bit-loading implemented and the constellation diagrams. In this proof-of-experiment, data rate of 7.813 Gbit/s per wavelength channel can be achieved. When decreasing the data rates, better BER can be obtained as shown in Fig. 5(c). The maximum data rate of the proposed system is limited by the optical signal to noise ratio (OSNR); hence as shown in Fig. 5(b), most of the subcarriers only have the modulation level of 3-bit.

4. Numerical Analysis

Numerical analysis using VPI Transmission Maker V7.5 is performed to evaluate the proposed RRF at even higher carrier frequencies. The simulation is based on the experimental parameters.

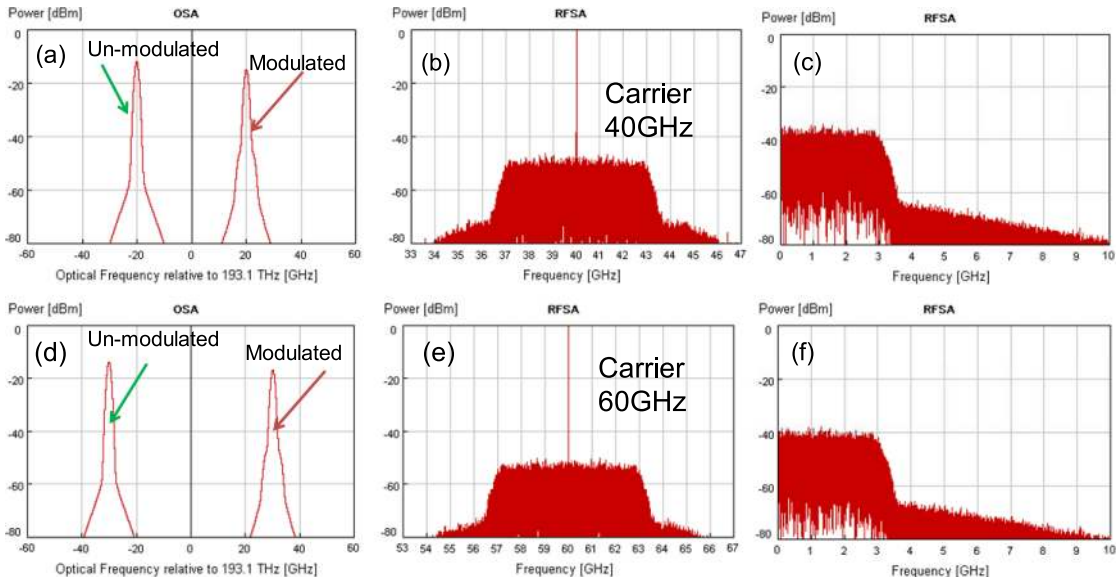

Fig. 6. Simulated optical spectra of (a) 40 GHz and (b) 60 GHz SSB ROF signals. Simulated RF spectra at carrier and baseband of (b) (c) 40 GHz and (e) (f) 60 GHz SSB ROF signals.

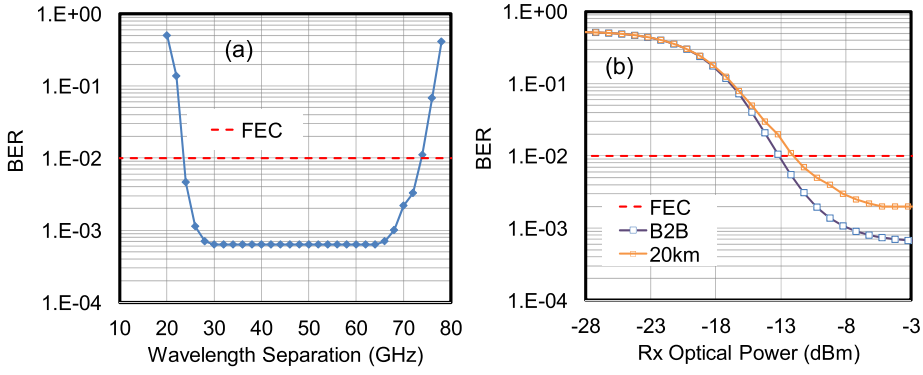

Fig. 7. Simulated BER performance of (a) the SSB ROF signals at different wavelength separations; and (b) the SSB 60 GHz ROF signal at B2B and after 20 km SMF transmission.

Fig. 6(a) and (d) show the optical spectra when the MZM is electrically driven at 20 GHz and 30 GHz respectively, and when one of the optical sidebands is encoded with OFDM signal via the MRM. When these SSB ROF optical signals are launched into a PD, the coherent beating between these two optical tones will produce the mm-wave ROF signal. Fig. 6(b) and (c) show the RF spectra at the 40 GHz carrier frequency and at the baseband, we can observe that there is a good match with the experimental results shown in Fig. 4(c) and (d). Fig. 6(e) and (f) show the RF spectra at the 60 GHz carrier frequency and at its baseband, and there is no observable difference between the 40 GHz ROF case.

Fig. 7(a) shows the simulated BER performance of the SSB ROF signal when the wavelength separation between the optical two tones is increased from 10 GHz to 80 GHz. We can observe that although the modulation bandwidth of the MZM is only 25 GHz, $>$60 GHz mm-wave generation can be supported without introducing BER degradation. Fig. 7(b) shows the BER at B2B and after 20 km SMF transmission of the SSB 60 GHz ROF signal, we can observe that a good transmission

performance can be achieved (∼1 dB of power penalty) when the ROF frequency is increased to 60 GHz.

5. Conclusion

Using analog ROF signal for mobile fronthaul network transmission is promising for future wireless networks. In this work, we proposed and demonstrated a SiPh based RRF for the mm-wave analog ROF systems. The proposed SiPh based RRF consisted of an integrated MZM and an MRM; producing a SSB 40 GHz mm-wave OFDM ROF signal, which is robust against fiber chromatic dispersion in the mobile fronthaul transmission. The RRF was fabricated using SiPh platform and could be potentially low-cost. 512 high split-ratios can be potentially achieved at the mobile fronthaul, facilitating the implementation of MIMO and CoMP techniques. Data rate of 7.813 Gbit/s per wavelength channel was achieved in the experiment. Numerical analysis was performed; and there are good matches of the simulation and experimental results for the SSB 40 GHz ROF case; and good simulation transmission performance can be observed when the ROF frequency is increased to 60 GHz.

References

[1] G. K. Chang and L. Cheng, "Fiber-wireless integration for future mobile communications," in *Proc. IEEE Radio Wireless Symp.*, 2017, pp. 16–18.

[2] 5G Spectrum Public Policy Position, 2017. [Online]. Available: https://www-file.huawei.com/-/media/CORPORATE/PDF/public-policy/public_policy_position_5g_spectrum.pdf?la=en

[3] J. Zhang, J. Yu, N. Chi, F. Li, and X. Li, "Experimental demonstration of 24-Gb/s CAP-64QAM radio-over-fiber system over 40-GHz mm-wave fiber-wireless transmission," *Opt. Exp.*, vol. 21, no. 22, pp. 26888–26895, 2013.

[4] C. Lim *et al.*, "Fiber-wireless networks and subsystem technologies," *J. Lightw. Technol.*, vol. 28, no. 4, pp. 390–405, Feb. 2010.

[5] C. T. Tsai, Y. C. Chi, P. C. Peng, and G. R. Lin, "Long-reach MMWoF using single-sideband modulated dual-mode VCSEL with 16-QAM OFDM at 8 Gbit/s," in *Proc. Opt. Fiber Commun. Conf. Exhib.*, 2017, Paper Tu2F.3.

[6] S. Liu, P. C. Peng, M. Xu, D. Guidotti, H. Tian, and G. K. Chang, "A long-distance millimeter-wave RoF system with a low-cost directly modulated laser," *IEEE Photon. Technol. Lett.*, vol. 30, no. 15, pp. 1396–1399, Aug. 2018.

[7] H. C. Chien, A. Chowdhury, Z. Jia, Y. T. Hsueh, and G. K. Chang, "60 GHz millimeter-wave gigabit wireless services over long-reach passive optical network using remote signal regeneration and upconversion," *Opt. Exp.*, vol. 17, pp. 3036–3041, 2009.

[8] C. W. Chow *et al.*, "Mitigation of signal distortions using reference signal distribution with colorless remote antenna units for radio-over-fiber applications," *J. Lightw. Technol.*, vol. 27, no. 21, pp. 4773–4780, Nov. 2009.

[9] C. W. Chow *et al.*, "100 GHz ultra-wideband (UWB) fiber-to-the-antenna (FTTA) system for in-building and in-home networks," *Opt. Exp.*, vol. 18, pp. 473–478, 2010.

[10] *C-RAN: The Road Towards Green RAN*, China Mobile, White Paper, Beijing, China, 2011.

[11] Alcatel-Lucent, "LightRadio network: A new wireless experience," White Paper, Boulogne-Billancourt, France, 2012.

[12] Nokia Siemens Networks, "Liquid radio: Let traffic waves flow most efficiently," White Paper, Espoo, Finland, 2011.

[13] J. Y. Sung, C. W. Chow, C. H. Yeh, Y. Liu, and G. K. Chang, "Cost-effective mobile backhaul network using existing ODN of PONs for the 5G wireless systems," *IEEE Photon. J.*, vol. 7, no. 6, Dec. 2015, Art. no. 7201906.

[14] A. Nirmalathas, P. A. Gamage, C. Lim, D. Novak, and R. Waterhouse, "Digitized radio-over-fiber technologies for converged optical wireless access network," *J. Lightw. Technol.*, vol. 28, no. 16, pp. 2366–2375, Aug. 2010.

[15] M. Zhu, L. Zhang, J. Wang, L. Cheng, C. Liu, and G. Chang, "Radio-over-fiber access architecture for integrated broadband wireless services," *J. Lightw. Technol.*, vol. 31, no. 23, pp. 3614–3620, Dec. 2013.

[16] Common Public Radio Interface; Interface Specification 2011, Aug. 2013. [Online]. Available: www.cpri.info

[17] Open Base Station Architecture Initiative; BTS System Reference Document, 2006. [Online]. Available: www.obsai.com

[18] C. Liu, J. Wang, L. Cheng, M. Zhu, and G. Chang, "Key microwave-photonics technologies for next-generation cloud-based radio access networks," *J. Lightw. Technol.*, vol. 32, no. 20, pp. 3452–3460, Oct. 2014.

[19] K. Xu *et al.*, "Microwave photonics: Radio-over-fiber links, systems, and applications [Invited]," *Photon. Res.*, vol. 2, pp. B54–B63, 2014.

[20] S. Liu, Y. M. Alfadhli, S. Shen, H. Tian, and G. K. Chang, "Mitigation of multi-user access impairments in 5G A-RoF-based mobile fronthaul utilizing machine learning for an artificial neural network nonlinear equalizer," in *Proc. Opt. Fiber Commun. Conf. Expo.*, 2018, Paper W4B.3.

[21] K. Yamada, J. Michel, M. Romagnoli, and H. K. Tsang, "Introduction for the group-IV photonics feature," *Photon. Res.*, vol. 2, p. GP1, 2014.

[22] R. Urata, H. Liu, C. Lam, P. Dashti, and C. Johnson, "Silicon photonics for optical access networks," in *Proc. Group IV Photon. Conf.*, 2012, Paper ThD1.

[23] S. Abrate *et al.*, "Silicon photonics and FDMA-PON: Insights from the EU FP7 FABULOUS project," in *Proc. Opt. Fiber Commun. Conf.*, 2015, Paper M3J.2.

[24] M. Glick, S. Rumley, G. Dongaonkar, Q. Li, K. Bergman, and R. Dutt, "Silicon photonic interconnection networks for data centers," in *Proc. IEEE Photon. Soc. Summer Topical Meeting Ser.*, Waikoloa, HI, USA, 2013, pp. 244–245.
[25] Y. Hsu *et al.*, "2.6 Tbit/s on-chip optical interconnect supporting mode-division-multiplexing and PAM-4 signal," *IEEE Photon. Technol. Lett.*, vol. 30, no. 11, pp. 1052–1055, Jun. 2018.
[26] *Soft-Decision FEC Benefits for 100G*, Fujitsu, Tokyo, Japan, 2012, pp. 1–3.
[27] L. Cheng *et al.*, "Coordinated multipoint transmissions in millimeter-wave radio-over-fiber systems," *J. Lightw. Technol.*, vol. 34, no. 2, pp. 653–660, Jan. 2016.
[28] T. C. Tzu *et al.*, "Equalization of PAM-4 signal generated by silicon microring modulator for 64-Gbit/s transmission," *J. Lightw. Technol.*, vol. 35, no. 22, pp. 4943–4948, Nov. 2017.